Controlled and Reversible Aggregation of Biotinylated Gold Nanoparticles with Streptavidin

Kadir Aslan,[†,§] Claudia C. Luhrs,[‡] and Víctor H. Pérez-Luna*[,†]

Department of Chemical and Environmental Engineering, Illinois Institute of Technology, 10 West 33rd Street, Chicago, Illinois 60616, and Departamento de Química, Universidad de Guadalajara, Boulevard Marcelino García Barragán No. 1451, Guadalajara, Jalisco 44430, México

Received: July 17, 2003; In Final Form: May 28, 2004

Biotinylated gold nanoparticles were prepared by using a two-step surface modification procedure. First, a carboxyl-terminated alkanethiol was chemisorbed onto the surface of gold nanoparticles in the presence of a stabilizing agent. Subsequently, the carboxyl groups were reacted with (+)-biotinyl-3,6,9,-trioxaundecanediamine and 2-(2-aminoethoxy)ethanol. This procedure resulted in stable, ligand-modified gold nanoparticles. Upon interaction with streptavidin, the biotinylated gold nanoparticles aggregated by means of specific biomolecular recognition. Their aggregation was studied by optical absorption spectroscopy. Controlled aggregation of biotinylated gold nanoparticles resulted in a shift in the surface plasmon resonance peak and broadening of the absorption spectrum of the nanoparticles. The spectral changes were used to assess the extent of aggregation. Aggregation was found to be dependent on the concentrations of streptavidin, biotinylated gold nanoparticles, and the surface mole fraction of biotin groups on the nanoparticles. Maximum aggregation was observed when 24 nM streptavidin and 0.80 nM biotinylated gold nanoparticles were used. Reversal of nanoparticle aggregation was accomplished by the addition of soluble biotin to the streptavidin−nanoparticle aggregates. Kinetic analysis of the absorbance data showed that streptavidin-induced aggregation of biotinylated gold nanoparticles could be interpreted in terms of a Reaction-Limited Colloidal Aggregation (RLCA) model. This indicates that optical absorption spectroscopy can provide a quantitative measurement of the aggregation process.

Introduction

Aggregation of metallic nanoparticles, induced by specific biomolecular interactions, is a practical tool for the development of simple colorimetric assays for the detection of DNA hybridization,[1−3] and has potential applications in immunoassays[4] and controlled-assembly of nanoparticles.[5] Gold nanoparticles are frequently used in a variety of applications due to their exceptional optical and electronic properties.[6−9] Their amenability for the attachment of biomolecules and ligands makes them a very attractive tool, especially for biosensing applications. Facile immobilization of biomolecules and ligands onto gold surfaces can be performed by means of thiol chemistry, which provides well-defined monolayers.[10] Aggregation of ligand-modified gold nanoparticles induced by specific biomolecular interactions can be characterized by optical absorption spectroscopy,[4] light scattering,[5,11a] small-angle X-ray scattering,[11b] and transmission electron microscopy.[5,11b]

Despite the promising progress in the development of aggregation-based immunoassays and controlled assembly of nanoparticles, certain issues such as nonspecific interactions of proteins with the nanoparticle surface and reversibility of the nanoparticle aggregation process have not been addressed completely.[4,5,11] In previous studies, the surface of gold nanoparticles was modified with short-chain precursor molecules and the stability of the nanoparticles was maintained by means of electrostatic stabilization.[4a,5,11] However, the precursor molecules used in such studies may not be effective at preventing nonspecific interactions. For example, they did not contain oligo(ethylene glycol) or other groups[12] that are very effective in preventing nonspecific interactions of proteins with surfaces. The fact that nonspecific adsorption of proteins could affect the sensitivity of immunoassays[4b] and result in irreversible and uncontrolled aggregation of the nanoparticles[4a,5,11] was not considered. Since such surface-modified gold nanoparticles were stabilized by means of electrostatic forces, their stability would be exceedingly dependent on the ionic strength and pH of the surrounding medium. This limits the use of surface-modified gold nanoparticles in a wider range of salt concentrations and pH values.[4a,5,11] Additionally, the reversibility of aggregation of biotinylated gold nanoparticles was not proved.[4,5,11] Reversal of aggregation by dissociating the adsorbed biomolecules might be beneficial for competitive dissociation assays.

We recently reported a method for the surface modification of gold nanoparticles with self-assembled monolayers (SAMs) using carboxylic acid terminated alkane thiols. Such particle preparations were stable within a wide range of pH (between pH 7 and 11).[13] Here, we investigate further functionalization of these carboxylic acid terminated gold nanoparticles with ligands that bind proteins by means of specific molecular recognition. We also describe their controlled and reversible aggregation via specific biomolecular interactions. Biotinylation of gold nanoparticles was performed according to Scheme 1. The biotin content on the surface of the nanoparticles can be

* Corresponding author. E-mail: perezluna@iit.edu. Phone: 312-567-3963. Fax: 312-567-8874.

† Illinois Institute of Technology.

‡ Universidad de Guadalajara.

§ Current Address: Institute of Fluorescence and Center for Fluorescence Spectroscopy, Medical Biotechnology Center, University of Maryland Biotechnology Institute, 725 West Lombard Street, Baltimore, MD 21201

10.1021/jp036089n CCC: $27.50
Published on Web 09/09/2004

SCHEME 1: Ligand Immobilization Procedure on Gold Nanoparticle Surfaces[a]

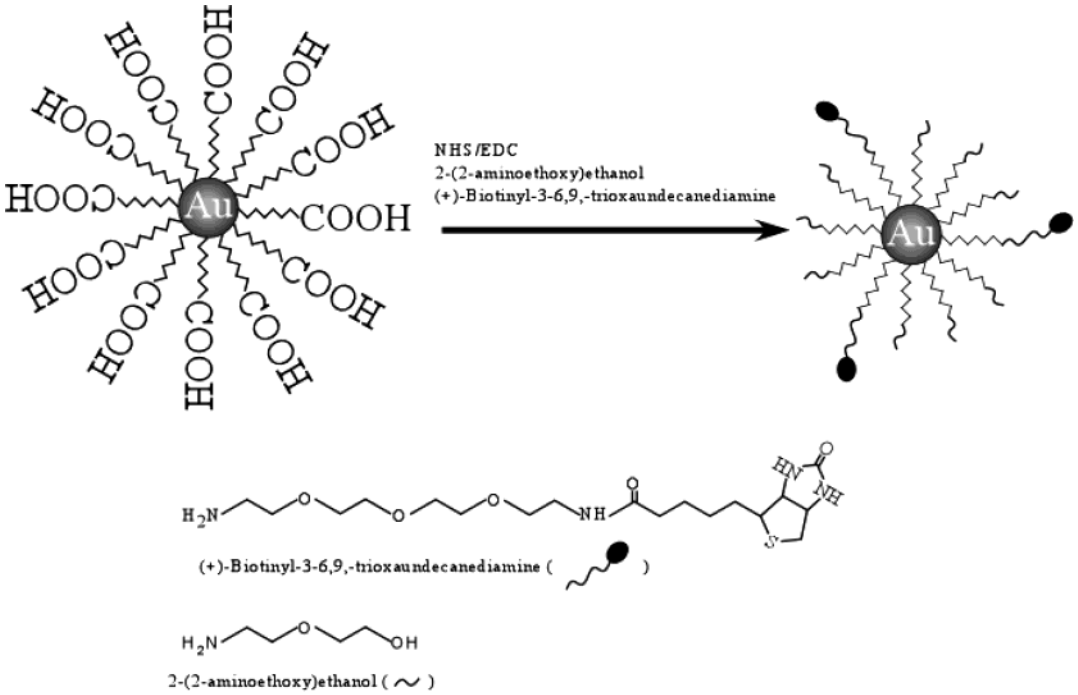

[a] Monolayer and metallic core not drawn to scale.

adjusted by varying the mole fraction of the two ligands in the reaction mixture (Scheme 1). To prevent nonspecific adsorption of proteins, to provide additional stability for the nanoparticle dispersions, and to provide optimal presentation of the biotin moieties, one of the ligands contained di(ethylene glycol) groups.

Experimental Section

Materials. Colloidal gold (monodisperse, 20 nm average particle diameter), streptavidin, *d*-biotin, hydrogen peroxide, sulfuric acid, sodium phosphate monobasic, Dulbecco's phosphate buffered saline (PBS), ethanol, 2-(2-aminoethoxy)ethanol (AEE), and *N*-hydroxysuccinimide (NHS) were obtained from Sigma. Polyoxyethylene (20) sorbitan monolaurate (Tween 20) and 16-mercaptohexadecanoic acid (16-MHDA) were obtained from Aldrich. (+)-Biotinyl-3,6,9,-trioxaundecanediamine (BA) was obtained from Pierce. *N*-3-(Dimethylaminopropyl)-*N*′-ethylcarbodiimide (EDC) was obtained from Fluka. All chemicals were used as received.

Buffers and Solutions. Sodium phosphate monobasic buffer solution was prepared to a 10 mM concentration at pH 7. Dulbecco's phosphate buffer saline (PBS) was dissolved in deionized water and its pH adjusted to 7.4. Exact pH values for buffer solutions were obtained with an Accumet AB15 pH meter. Deionized water (electric resistivity >18 MΩ·cm) was obtained from a Barnstead Nanopure Infinity UV/UF water purification system. All glassware used was treated with "piranha solution" (3:7 30% hydrogen peroxide/concentrated sulfuric acid: **CAUTION!** piranha solution reacts violently with most organic materials and should be handled with extreme care).

Solutions of 0.50 mM 16-MHDA were prepared in degassed ethanol. Tween 20 solutions were prepared in degassed sodium phosphate buffer at pH 7.

Surface Modification of Gold Nanoparticles. The facile immobilization of ligands on gold nanoparticles was performed with the following steps: (1) chemisorption of a long-chain carboxyl-terminated alkane thiol (MHDA) on gold nanoparticles as described before,[13] (2) the activation of surface carboxyl groups with EDC and NHS, and (3) the covalent coupling of ligands (Scheme 1). The stability of the system during surface modification was assessed by using optical absorption spectroscopy.

Gold nanoparticle dispersions with a concentration of 0.80 nM (determined by measuring absorbance at 520 nm and using an extinction coefficient of 1.25×10^9 M^{-1} cm^{-1}) were degassed with nitrogen gas before use. Equal volumes (400 μL) of gold nanoparticle dispersions (0.80 nM, before mixing) and Tween 20 (1.82 mg/mL, before mixing) in pH 7 buffer were gently mixed and allowed to stand for at least 30 min to allow for monolayer physisorption of Tween 20 to the gold nanoparticles to be completed.[13] Then, 400 μL of 0.50 mM 16-MHDA was added and the final mixture (final concentrations: [gold nanoparticles] = 0.27 nM, [Tween 20] = 0.61 mg/mL, [16-MHDA] = 0.17 mM) was allowed to stand for a minimum of 3 h for the chemisorption of 16-MHDA to be completed on gold nanoparticles.[13] To remove excess 16-MHDA and Tween 20, the final mixture was centrifuged (three times for 15 min at 15 700 g; the supernatants were discarded after each cycle) and resuspended in phosphate buffer (with 1.82 mg/mL Tween 20 at pH 7). After a final centrifugation step, the 16-MHDA modified-gold nanoparticles in the centrifugate were reacted with a mixture of freshly prepared 50 mM NHS and 200 mM EDC solution (in phosphate buffer without Tween 20) for 5 min. The resulting nanoparticle dispersion was centrifuged (5 min, 15 700 g) and the centrifugate was then resuspended in sodium phosphate buffer containing 1.82 mg/mL of Tween 20 at pH 7, then centrifuged again (5 min, 15700 g). After discarding the supernatant, the remaining NHS ester−alkanethiol modified-gold nanoparticles were reacted with a freshly prepared solution of AEE (22 mM) and BA (2.4 mM) for 10 min. Excess BA and AEE were removed by use of Microcon 30 (MW cutoff 30 000) centrifugal filters for 5 min at 6000 g (at least three times). The retentate that contained biotinylated gold nanoparticles was centrifuged (5 min, 15 700 g) and resuspended in

sodium phosphate buffer containing 1.82 mg/mL of Tween 20 at pH 7 and centrifuged again. The centrifugate containing the biotinylated gold nanoparticles was then stored at 4 °C for future use. We found that this procedure was sufficient to remove unreacted biotinylated ligands by testing the aggregation induced in low concentrations of streptavidin preparations. All solutions having gold nanoparticles were stored in polypropylene centrifuge tubes in the dark to prevent light-induced flocculation of the nanoparticles and oxidation of the alkane thiols.[14]

Characterization Techniques. *Optical Absorption Spectroscopy*. The optical absorption spectra of all samples were recorded with a Shimadzu UV-2401PC dual-beam spectrophotometer, using 1-cm path length quartz cuvettes.

Transmission Electron Microscopy (TEM). TEM images were obtained on a JEOL model 1010 that was operated at 100 kV. The samples for TEM analysis were prepared by evaporation of droplets placed on Formvar-carbon TEM grids. An objective aperture for contrast effects was also used.

X-ray Photoelectron Spectroscopy (XPS). The surfaces of the nanoparticles were analyzed with a Surface Science Instruments model SSX-100 spectrometer at the National ESCA and Surface Analysis Center for Biomedical Applications (NESAC/BIO) at the University of Washington. Nanoparticle dispersions in DI water were evaporated on the surface of clean silicon in order to analyze their surface chemistry.

Survey scans from 0 to 1000 eV binding energy were performed to determine the elemental composition of the nanoparticles. High-resolution scans of carbon (C1s), oxygen (O1s), and nitrogen (N1s) were also recorded, using 20 eV window resolution. An Al $K\alpha_{1,2}$ monochromatized X-ray source ($h\nu = 1486.6$ eV) was used to stimulate photoelectron emission. The residual pressure in the analysis chamber was on the order of 10^{-9} Torr or lower during spectral acquisition. The spectral envelopes were resolved into Gaussian peaks to fit the spectra and the hydrocarbon C1s peak was referenced at 284.6 eV.

Determination of Aggregation with Flocculation Parameter. The aggregation of biotinylated gold nanoparticles was quantified by a semiempirical flocculation parameter, introduced elsewhere.[13−15] The flocculation parameter is defined as the integrated absorbance between 600 and 800 nm of the optical absorption spectra normalized to the absorption intensity of the surface plasmon peak. Briefly, this number increases with the degree of aggregation of the gold nanoparticles in agreement with theoretical principles based on the presence of transversal and longitudinal surface plasmons that occur upon aggregation.[14]

Results and Discussion

Immobilization of Ligands on Gold Nanoparticles. Figure 1 shows the normalized optical absorption spectra of gold nanoparticles before and at each step of the biotin derivatization procedure. The surface plasmon resonance peak of gold nanoparticles occurs at 520 nm as expected. A shift to 525 nm is observed upon functionalization with 16-MHDA (the spectrum was taken after the separation of excess 16-MHDA and Tween 20 by centrifugation and resuspension of nanoparticles in buffer solution). This results from the chemisorption of thiol molecules to the nanoparticle surface. The shift in the SPR peak was not accompanied with marked broadening of the spectrum. Lack of broadening of the spectrum indicates that gold nanoparticles do not aggregate upon chemisorption of alkanethiol. However, when 16-MHDA-modified gold nanoparticles are reacted with NHS and EDC to form active surface NHS esters, the SPR peak shifted and broadened dramatically. This clearly indicated aggregation of nanoparticles and was due to the loss of surface

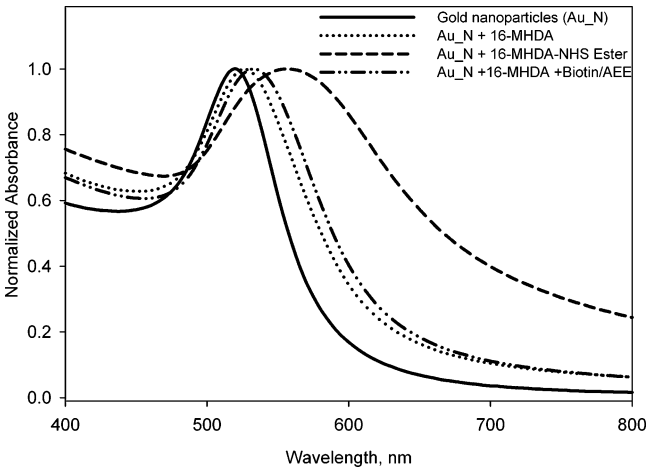

Figure 1. Normalized optical absorption spectra of gold nanoparticles at each step of the ligand immobilization procedure.

charges upon formation of active esters. The surface NHS esters do not carry any charges, and thus gold nanoparticles experience mostly attractive van der Waals forces because repulsive electrostatic forces are eliminated. In the next step, where the ligands (BA and AEE) are covalently attached to carboxyl groups of the alkane thiol, the SPR peak shifts back to 531 nm with a concomitant narrowing of the spectrum, indicating redispersion of the nanoparticles. The restored stability upon reaction with these ligands can be attributed to the presence of oligo(ethylene glycol) moieties in the ligand chains which create repulsive forces between the nanoparticles by means of steric hindrance. The difference in the SPR peak between unmodified gold nanoparticles and biotinylated gold nanoparticles, which changed from 520 to 531 nm, is due to the local increase in the refractive index caused by the addition of ligand layers to the surface of gold nanoparticles.[14−19] TEM images of the unmodified gold nanoparticles with Tween 20 and biotinylated gold nanoparticles show that both samples were well dispersed and that core fusion did not occur (Figure 2). This is in agreement with the lack of broadening of the SPR peak observed by optical absorption spectroscopy. Thus, this method produces individual (nonaggregated) and stable biotinylated gold nanoparticles.

The effectiveness of the surface modification procedure employed here, in terms of preserving the stability of the nanoparticles while modifying their surfaces, lies in the presence of Tween 20 in buffer solutions that were used for the resuspension of gold nanoparticles after centrifugation steps.[13] When Tween 20 was not present in buffer solutions, gold nanoparticles aggregated irreversibly and the particles precipitated. We also determined that "aging" of unmodified gold nanoparticles results in slow, irreversible aggregation of the nanoparticles that can be prevented when the nanoparticles are stored in phosphate buffer (pH 7) containing Tween 20.[13]

Elemental analysis of the biotinylated gold nanoparticles was done by X-ray photoelectron spectroscopy. The data revealed the presence of carbon, nitrogen, oxygen, gold, and silicon (from the substrate where the nanoparticles were deposited) (Table 1). The presence of large amounts of oxygen and silicon in the sample is attributed to the pretreatment of silicon wafers with "piranha solution" that creates silicon oxide on the wafer surface. Mixed layers of ligands that adsorbed on the surface of the gold nanoparticles contributed only to oxygen, carbon, sulfur, and nitrogen. However, the exact amount of sulfur could not be determined because of the small signal. A series of narrow scans in the C1s, O1s, and N1s binding energy regions were recorded and the C1s results are presented in Table 2. The binding

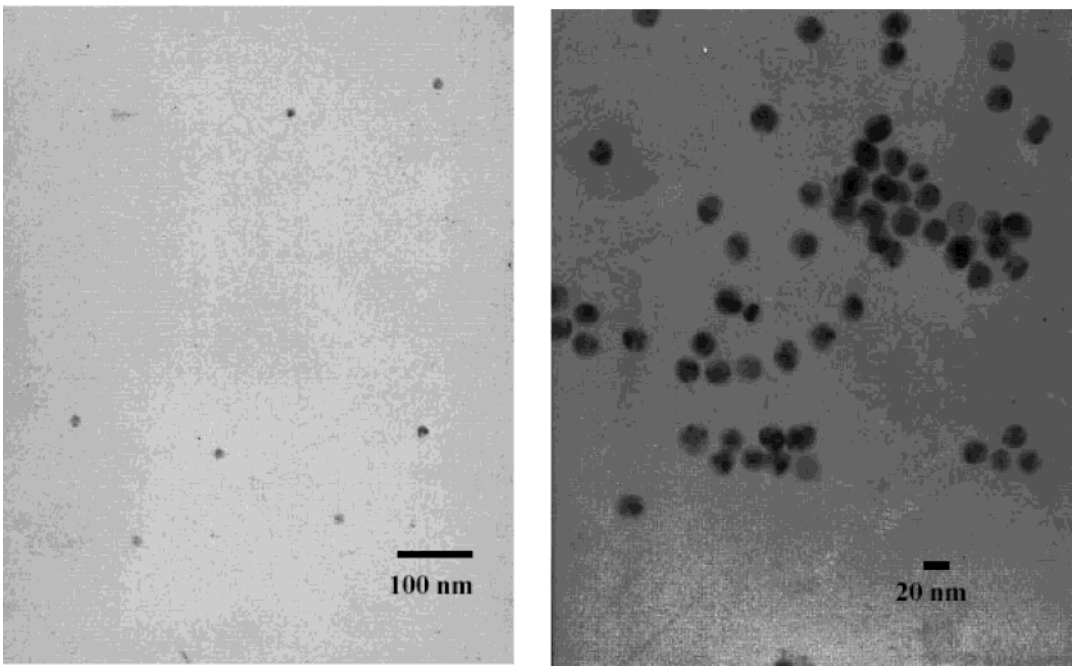

Figure 2. TEM images of (A) unmodified gold nanoparticles stabilized with Tween 20 and (B) biotinylated gold nanoparticles.

TABLE 1: Elemental Percentages of Biotinylated Gold Nanoparticles Obtained by XPS (Mole Fraction of Biotin is 0.10 in Solution)

% C	% N	% O	% Au	% Si
45.1	0.9	28.0	2.9	23.1

TABLE 2: Binding Energies (eV) for Core-Level Electrons of Mixed Layers

	C1s			
	N−(C═O)−N	N−C═O	C−O, C−N	CH_x
binding energy, eV	289.0	287.6	286.1	284.6

energies were found to be in agreement with the values reported in the literature.[20a] The C1s peak was resolved into four peaks due to four different carbon species, $-CH_x-$, C−O, or C−N, O═C−N, and N−(C═O)−N. These results confirm that BA and AEE successfully reacted with the terminal carboxyl group of the 16-MHDA and that the stable nanoparticle preparations obtained are indeed functionalized with biotin.

Streptavidin-Induced Aggregation of Biotinylated Gold Nanoparticles. Aggregation of ligand-functionalized gold nanoparticles in the presence of a multivalent ligand-binding protein depends on (1) the frequency of collisions between the protein and the ligand-functionalized gold nanoparticles and (2) the affinity of ligand−protein interactions. Since the biomolecular interaction between streptavidin and biotin is one of the strongest ($K_a \approx 10^{13}$ M^{-1}) found in nature,[21] we assume that streptavidin-induced aggregation of biotinylated gold nanoparticles is dominated by the collision frequency of the nanoparticles and streptavidin molecules. The extent of these collisions is directly related to the concentrations of biotinylated gold nanoparticles and streptavidin in solution. The aggregation process begins with the binding of streptavidin to a biotin moiety on the gold nanoparticle surface. Once this occurs, a competition for available biotin sites ensues between free streptavidin and streptavidin already bound to another gold nanoparticle. The aggregate grows only when a biotin group on one gold nanoparticle binds with a streptavidin molecule that is already bound to a different gold nanoparticle. Large amounts of streptavidin eventually lead to saturation of the biotin sites on a growing aggregate. Once all of the biotin groups on all of the growing aggregates are saturated, aggregation stops, resulting in finite size aggregates. Therefore, the aggregation process can be both initiated and inhibited by free streptavidin.

Effect of the Concentration of Biotinylated Gold Nanoparticles on the Aggregation Process. Since streptavidin molecules have two pairs of biotin binding sites on opposite sides of the molecule, *at least* two different biotinylated gold nanoparticles can be cross-linked with a single streptavidin molecule resulting in aggregation of the nanoparticles (Scheme 2A). Aggregation of gold nanoparticles leads to additional surface plasmon bands at longer wavelengths than those for individual nanoparticles because the vibrations of free electrons in individual nanoparticles became electronically coupled to each other.[22,23] After the coupling of nanoparticles, the oscillating electrons in one nanoparticle experience the electric field due to the oscillations of the free electrons in a second nanoparticle, which leads to a collective plasmon oscillation of the aggregated system. The frequency and intensity of the latter depend on the degree of aggregation as well as the orientation of the individual nanoparticles within the aggregate.[22,23] This manifests in broadening of the optical absorption spectrum and increased flocculation parameter. To follow the kinetics of aggregation, we monitored the changes in absorbance at 600 nm with respect to time. Upon aggregation, the broadening of the spectra results in marked increased absorbance at this wavelength that allows real time monitoring of the fast aggregation process.

To observe the effect of concentration of biotinylated gold nanoparticles on streptavidin-induced aggregation, we performed experiments where a fixed amount of streptavidin was allowed to interact with biotinylated gold nanoparticles at various concentrations. Figure 3 shows the change in absorbance (ΔA_{600}) of biotinylated gold nanoparticles (0.25−1.00 nM) at 600 nm with respect to time after the addition of streptavidin (10 nM in the final mixture). This increase proceeded at different rates, and the total amount of change in absorbance varied with the concentration of biotinylated gold nanoparticles (Figure 3, inset). The maximum amount of change in absorbance is denoted as $\Delta A_{600,max}$ and it is the final ΔA_{600} value after the signal leveled out (when 1.00 nM biotinylated gold nanoparticles were used

SCHEME 2: Schematic Representation of Possible Interactions of Streptavidin with Biotinylated Gold Nanoparticles. Addition of Streptavidin to Biotinylated Gold Nanoparticles Can Result in Monolayer Coverage of Streptavidin on the Surface of the Nanoparticles, or it Can Induce Nanoparticle Aggregation. (A) Addition of Soluble Biotin Leads to Dissociation of Streptavidin with Subsequent Disaggregation. (B) If Streptavidin is Saturated with Soluble Biotin it Does Not Interact with the Biotinylated Gold Nanoparticles.

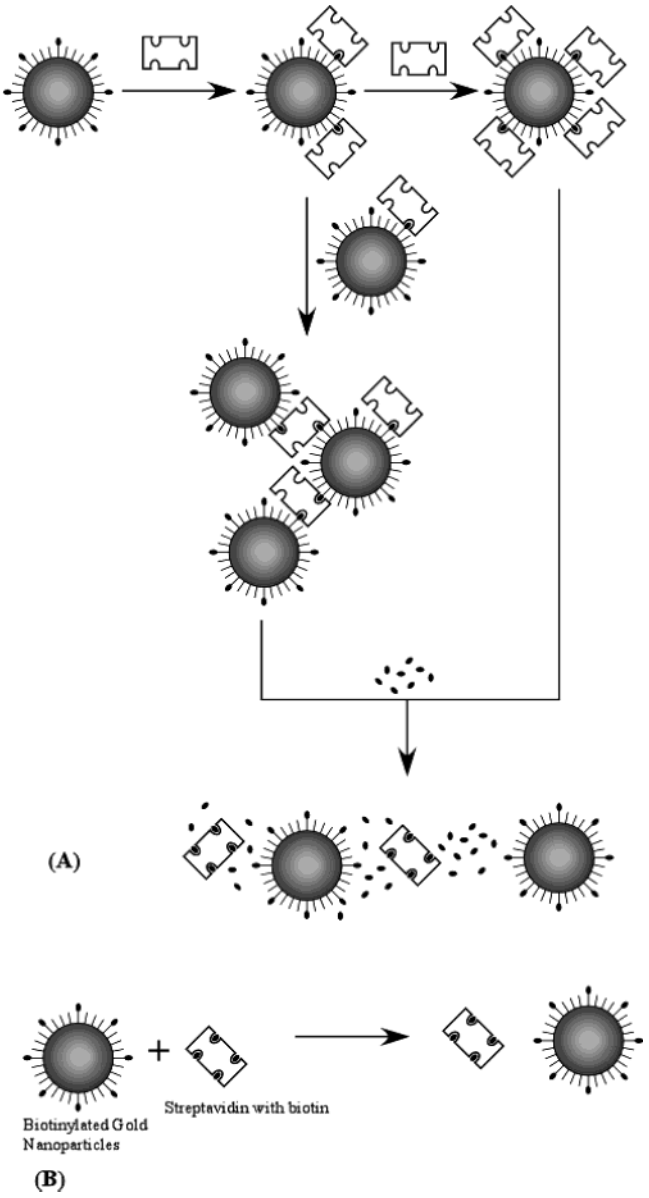

it took 9000 s for the signal to level out but only the time progression up to 3000 seconds is reported). The initial rate of change in absorbance is defined by the slope of the linear region of the initial ΔA_{600} versus time plot. The slope and the total change in the absorbance were the smallest when the concentration of gold nanoparticles was 0.25 nM. As the concentration of biotinylated gold nanoparticles increased, both $\Delta A_{600}/\Delta t$ and $\Delta A_{600,max}$ increased until 0.80 nM. When 1.00 nM biotinylated gold nanoparticles was used, the initial rate decreased and longer time was needed for the signal to level out; however, $\Delta A_{600,\,max}$ was larger. We note that for gold nanoparticle concentrations larger than 0.80 nM, absorbance values higher than 1.00 were obtained. We performed the rest of the experiments with a

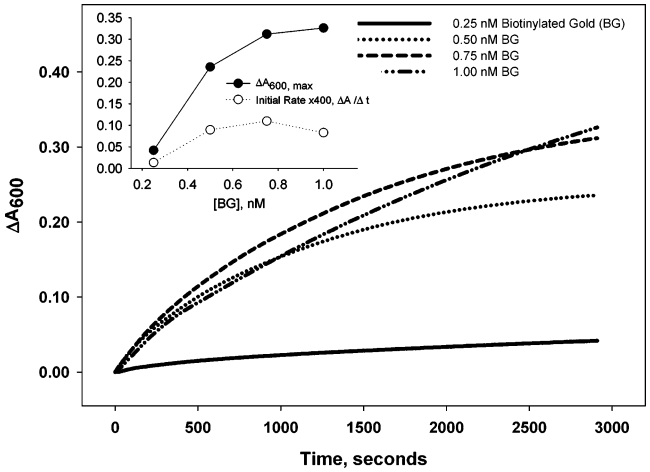

Figure 3. Change in absorbance of biotinylated gold nanoparticles at 600 nm with respect to time after the addition of streptavidin (10 nM in the final solution). Inset: Total amount of change in the absorbance at 600 nm ($\Delta A_{600,max}$) and the initial rate of change in absorbance ($\Delta A_{600}/\Delta t$) versus concentration of biotinylated gold nanoparticles.

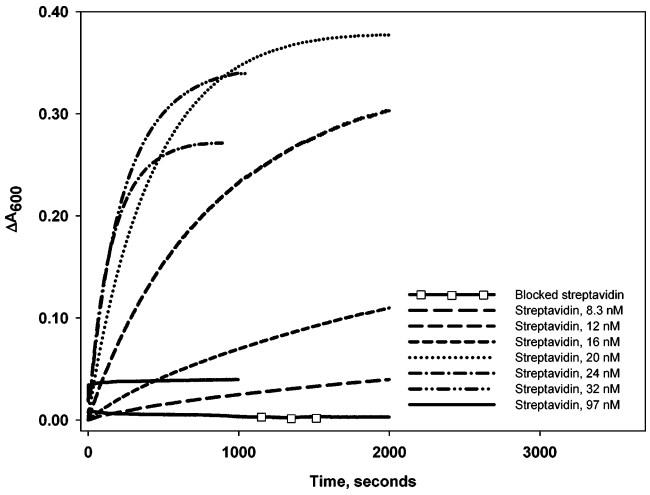

Figure 4. Change in absorbance of 0.80 nM biotinylated gold nanoparticles at 600 nm with respect to time after the addition of various amounts streptavidin.

concentration of biotinylated gold nanoparticles of 0.80 nM in the final mixture considering that this would result in absorbance values close to 1.00 and the fact that faster aggregation occurred with this concentration.

Effect of the Concentration of Streptavidin on the Controlled Aggregation of Biotinylated Gold Nanoparticles. To investigate the extent of aggregation of biotinylated gold nanoparticles when the concentration of streptavidin was varied, experiments with 0.80 nM biotinylated gold nanoparticles and 4−200 nM streptavidin were conducted. Figure 4 shows the change in absorbance of biotinylated gold nanoparticles at 600 nm with respect to time after the addition of different amounts of streptavidin. Control experiments (Scheme 2B), where the binding sites of streptavidin were saturated with soluble biotin prior to interaction with biotinylated gold nanoparticles, showed that addition of blocked streptavidin to biotinylated gold nanoparticles did not change the absorbance of the system other than that due to dilution effects. However, when streptavidin with unblocked binding sites was allowed to interact with biotinylated gold nanoparticles, there was a considerable amount of change in the absorbance of the biotinylated gold nanoparticles due to aggregation. These observations proved that the surface composition of these biotinylated gold nanoparticles

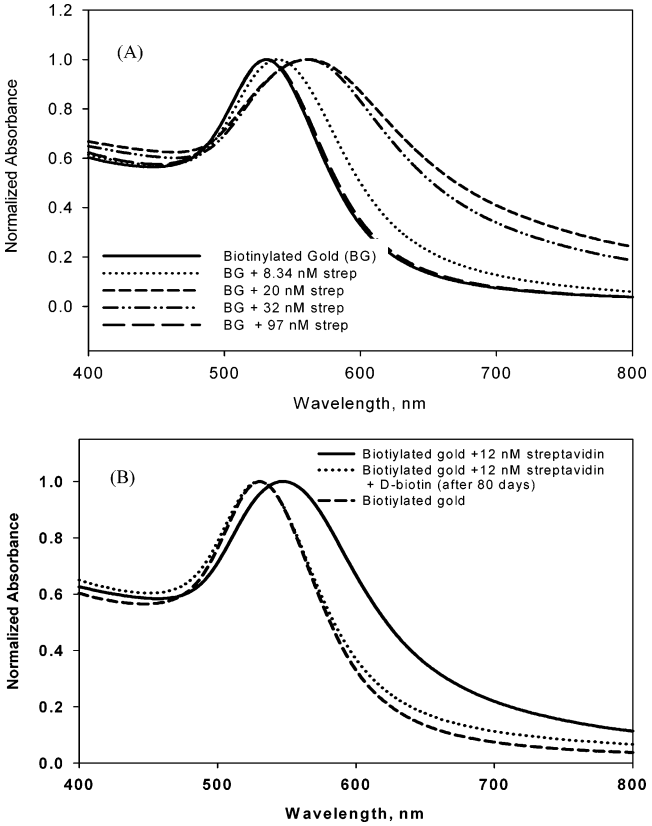

Figure 5. Normalized optical absorption spectra of 0.80 nM biotinylated gold nanoparticles before and after addition of different amounts of streptavidin and (B) normalized optical absorption spectra of 0.80 nM biotinylated gold nanoparticles before and after addition of 12 nM streptavidin and after the addition of 1 mM soluble biotin.

prevents nonspecific interaction of streptavidin with the nanoparticles and allows only specific interaction to occur between surface-bound biotin and streptavidin.

Figure 5A shows the normalized optical absorption spectra of biotinylated gold nanoparticles before and after addition of different amounts of streptavidin (only selected spectra are shown for clarity). The SPR peak of biotinylated gold nanoparticles occurs at 531 nm as indicated earlier. A shift to 538 nm is observed upon addition of 8.0 nM streptavidin accompanied by little broadening. However, addition of 20 and 32 nM streptavidin caused significant broadening and a shift in the SPR peak to 560 nm. Large concentrations of streptavidin (97 nM) did not cause significant changes in the SPR peak and the spectrum did not broaden. This indicated that a large excess of streptavidin blocks all the available biotin groups, thus limiting the extent of aggregation. We also checked the reversibility of the interaction between nanoparticle-immobilized biotin and streptavidin. Soluble biotin was added to streptavidin aggregated biotinylated gold nanoparticle and after 80 days their spectra were acquired to determine the reversibility of aggregation. As shown in Figure 5B, the addition of soluble biotin reverses the aggregation process by dissociating the streptavidin molecules from the surfaces so that the SPR peak returned to its original position as in nonaggregated biotinylated gold nanoparticles. The absorption spectra (Figure 5) were used to semiquantitatively determine the extent of aggregation by integrating the absorbance between 600 and 800 nm (flocculation parameters).

Figure 6 shows the flocculation parameters calculated from the normalized absorption spectra of biotinylated gold nanoparticles after their interaction with streptavidin and soluble

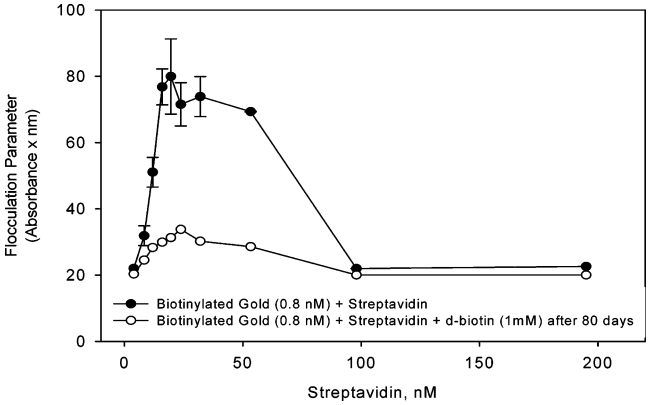

Figure 6. Flocculation parameter versus streptavidin concentration for biotinylated gold nanoparticles after the addition of streptavidin and soluble biotin.

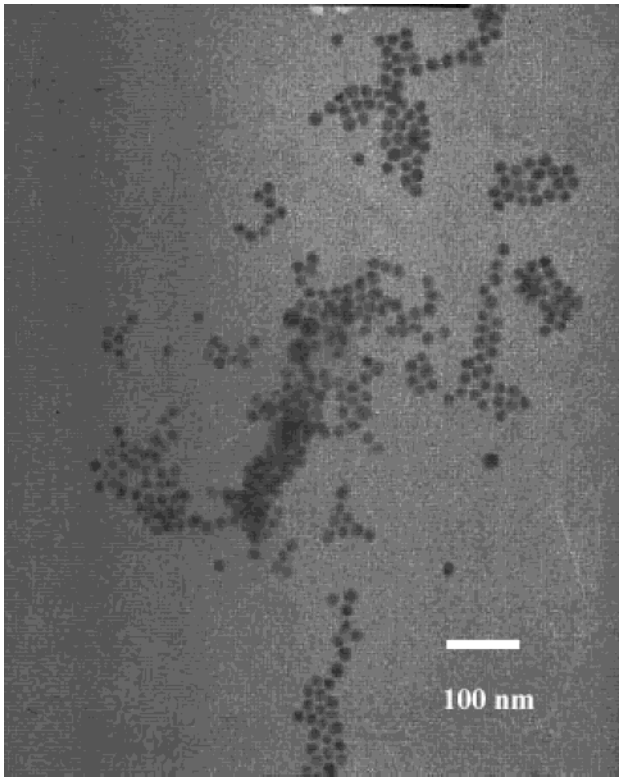

Figure 7. Transmission electron microscope image of biotinylated gold nanoparticles after addition of streptavidin (8 nM).

biotin versus the concentration of streptavidin used. The flocculation parameter initially increased (up to 20 nM of streptavidin) and decreased thereafter. The flocculation parameter decreased significantly after the addition of soluble biotin to the nanoparticle/streptavidin aggregates, indicating reversal of the aggregation process.

Figure 7 shows a TEM image of aggregates of biotinylated gold nanoparticles when 8.0 nM streptavidin was used. It is observed that the biotinylated gold nanoparticles are organized in aggregates with similar distances separating the individual nanoparticles from one another. Similar separation distances were obtained because one streptavidin molecule links two nanoparticles. This is microscopic evidence that streptavidin interacts with biotin groups on the surface, mediating the aggregation of nanoparticles, and further confirms the hypothesis of protein-induced aggregation.

The streptavidin-induced aggregation of biotinylated gold nanoparticles can be rationalized by considering the molecular

characteristics of streptavidin and the conditions under which biotin−streptavidin interactions take place. Streptavidin molecules can cross-link *at least* two different biotinylated gold nanoparticles so that nanoparticle aggregation results. However, in order for the cross-linking to occur the ratio of available biotin groups to binding sites must not be significantly different from 1, as the resultant shortage/excess will cause the aggregation to stop. For example, if the amount of streptavidin in solution was greater than that required for monolayer coverage on the surface of gold nanoparticles, negligible aggregation would occur due to inaccessibility of the remaining biotin groups.[11b] Conversely, if the amount of streptavidin is very small, the extent of aggregation is limited by the amount of streptavidin that can bridge two nanoparticles or aggregates. Thus, the maximum amount of streptavidin that will induce significant aggregation is limited by the surface area required for binding.

The following simple calculations allow us to obtain an estimate of the amount of protein that will induce significant aggregation. The projected surface area of streptavidin is approximately 20 nm^2 (the dimensions of a streptavidin molecule are $4 \times 4 \times 5$ nm).[24] The surface area of a single gold nanoparticle is 1520 nm^2 (based on a diameter of 22 nm considering the monolayer of ligands around the nanoparticle). Thus, a single nanoparticle could bind a maximum of 76 streptavidin molecules if a close-packed monolayer was formed. However, the random nature of protein adsorption limits the number of streptavidin molecules that could adsorb on the surface of the biotinylated gold nanoparticles to 42 (based on random sequential adsorption theory).[25] This corresponds to 33 nM streptavidin when 0.80 nM biotinylated gold nanoparticles is used. This is in close agreement with the data shown in Figure 6. In fact, the aggregation of nanoparticles begins to decrease at concentrations of streptavidin larger than 32 nM. Figure 6 also shows maximum aggregation of biotinylated gold nanoparticles when 20 nM streptavidin (3/5 of the concentration required for monolayer coverage) was used. In a previous study, Connolly et al.[11b] made similar observations on streptavidin-induced aggregation of disulfide desthiobiotin modified gold nanoparticles (7.6 nm in diameter) in a flow mixing system studied by dynamic light scattering (DLS). Their findings of average hydrodynamic radius of aggregated gold nanoparticles versus surface area equivalents (or concentration) showed a maximum in the radius of the aggregated nanoparticles at around one-half of the concentration of streptavidin needed for monolayer coverage.[11a]

These results show that aggregation, as measured in terms of the average hydrodynamic radius,[11] could also be related to the information provided by the flocculation parameter.[13−15] Given that aggregation of metallic nanoparticles leads to additional resonances occurring at longer wavelengths and that the flocculation parameter is the integration of these resonances, it is reasonable to assume that the magnitude of the flocculation parameter is closely related to the size of nanoparticle aggregates. However, the dependency of the flocculation parameter on aggregate sizes is not known. To analyze the aggregation process we make the assumption that *the extinction coefficient per individual nanoparticle at wavelengths larger than the plasmon band of nonaggregated particles increases in direct proportion to the number of particles in an aggregate*. Although this assumption may not hold for small aggregates, it is reasonable to expect that the extinction coefficient per particle reaches an asymptotic value for large aggregates. Thus, if the aggregation process proceeds such that small particle aggregates exist only for a brief period of time before they get incorporated in the larger aggregates it may be a reasonable assumption to make in order to analyze the kinetics of aggregation by optical absorption spectroscopy.

The mole fraction of biotin groups on the surface of the gold nanoparticles was equal to 0.24 as determined by XPS. This number was calculated from the N1s signal of nanoparticles with mixed BAA/AEE moieties as compared to nanoparticles derivatized with 100% AEE or BA. Making an analogy to SAMs on flat surfaces, where the alkanethiolates cover an area of 0.21 nm^2 on gold surfaces,[10] the number of alkanethiolates is expected to be approximately 7240 per nanoparticle. This corresponds to 1390 biotin groups per nanoparticle (assuming that both ligands have a similar rate of reaction and 80% yield of reaction[20b]) and 33 biotin groups per streptavidin molecules. Since there are 33 biotin groups available for every streptavidin molecule on the surface of the nanoparticles, we assume that the effect of surface biotin concentration on the adsorption of streptavidin is insignificant provided that steric hindrance due to molecular crowding does not interfere with binding.

Kinetic Analysis of the Interactions between Biotinylated Gold Nanoparticles and Streptavidin. The interactions of biotinylated gold nanoparticles and streptavidin involve two processes: (I) adsorption of streptavidin onto biotinylated gold nanoparticles and (II) cross-linkage of biotinylated gold nanoparticles by streptavidin (Scheme 2A). Our hypothesis is that adsorption of streptavidin initially occurs faster than cross-linking of the nanoparticles. That is, the interaction between a biotinylated nanoparticle and a streptaviding molecule is far more likely to occur during the initial stages than cross-linking of two nanoparticles (or clusters of nanoparticles) because of the large differences in the diffusion coefficients of single nanoparticles and nanoparticles aggregates. Additionally, we observe from Figure 4 that when a high concentration of streptavidin (97 nM) is used, the total increase in absorbance, ΔA_{600}, is relatively small compared to curves obtained with smaller concentrations of streptavidin. This result implies that aggregation of nanoparticles is negligible at such large concentrations of streptavidin (see also Figure 6) and in this case ΔA_{600} mostly reflects the adsorption of streptavidin. Conversely, if aggregation is significant, ΔA_{600} will largely reflect aggregation effects. Because the contribution of streptavidin adsorption to ΔA_{600} is much smaller than that due to aggregation we can perform an analysis of the aggregation process based on our measured changes in absorbance by fitting our data to aggregation models reported elsewhere.[26]

Kinetic Analysis of the Controlled Aggregation of Biotinylated Gold Nanoparticles. The aggregation data obtained from optical absorption spectroscopy were analyzed with two kinetic models[26,27] describing the aggregation of colloidal particles based on Smoluchowski kinetics.[28] In both models, the extent of aggregation is described by the mean number of bonds per nanoparticle in an aggregate if only one bond between two nanoparticles is counted and cyclic structures are not allowed.[27]

The first model is based on diffusion-limited colloidal aggregation, where effective collisions between two small aggregates, two large aggregates, or a small and a large aggregate are equally likely to occur.[26,27] In this model, the extent of aggregation, as determined by the average number of bonds per particle, b_{cnst}, in an aggregate is given by[27]

$$b_{cnst} = \frac{t/\tau_{cnst}}{1 + t/\tau_{cnst}} \quad (1)$$

where the subscript cnst indicates that the extent of aggregation,

b_{cnst}, is obtained by assuming an equal probability of effective collisions between aggregates regardless of their size. The parameter τ_{cnst} is called the aggregation time constant and is related to the concentration of particles per volume, N_0, and the constant reaction kernel for collisions between aggregates, A, as follows

$$1/\tau_{cnst} = \frac{AN_0}{2} \tag{2}$$

The second model is based on reaction-limited colloidal aggregation, where effective collisions are more likely between two large aggregates than between two small aggregates. In this model, the extent of aggregation is given by[27]

$$b_{sum} = b_\infty(1 - e^{-t/\tau_{sum}}) \tag{3}$$

This model assumes a reaction kernel that depends on the sum of the sizes of aggregates colliding to form a larger aggregate. Here, τ_{sum} also indicates the aggregation time constant and it is proportional to the concentration of particles per unit volume, N_0.

$$1/\tau_{sum} = BN_0 \tag{4}$$

The parameter B is a measure of the probability that a single particle on one cluster will react with another particle on a different cluster.[27]

These models are based on the assumption that the protein coats the nanoparticles immediately upon mixing, and that the protein-coated nanoparticles then act as aggregating particles. These conditions are likely to be met for streptavidin-mediated aggregation of biotinylated gold nanoparticles if we consider the large differences in size between a streptavidin molecule (4−5 nm) and a nanoparticle (or nanoparticle aggregates) with bound streptavidin (>20 nm). When free streptavidin is present in the system, its collision with nanoparticles or aggregates is more likely to occur because of its small size (larger diffusion coefficient) than collision between aggregates or nanoparticles containing streptavidin.

The extent of aggregation of nanoparticles (b_{cnst} or b_{sum}) is usually determined by using size measurement techniques such as light scattering,[27] small-angle X-ray scattering, and/or TEM. However, optical absorption spectroscopy could provide a more accessible technique for the analysis of aggregation kinetics of gold nanoparticles. As mentioned earlier, aggregation of nanoparticles occurs when *at least* two different nanoparticles are cross-linked by the same streptavidin molecule. These nanoparticle aggregates could be in the form of dimers, trimers, and other larger forms, and as they grow in size, the observed extinction coefficient (or absorbance) at longer wavelengths increases due to the coupled collective plasmon oscillations.[14,22,23] The absorbance values measured at these wavelengths are the average values of the absorbance of all the nanoparticle aggregates. These have been used for semiquantitative determination of the aggregation.[14,15] If the change in absorbance at a certain wavelength (e.g., 600 nm) could be related directly to the extent of aggregation, b, this would allow for quantitative analysis of the aggregation process (as b increases, the absorbance of the nanoparticles at 600 nm increases). The following analysis is thus made by assuming that the extent of aggregation, b, is proportional to the change in absorbance, ΔA_{600}.

Figure 8 shows the change in absorbance at 600 nm with respect to time for 24 nM streptavidin (experimental data), the model fit by using diffusion limited colloidal aggregation (eq 1), and the model fit by using reaction limited colloidal aggregation (eq 3). The single exponential model closely fitted the experimental data ($r^2 = 0.999$), while the model based on diffusion-limited aggregation failed to fit the data. Analysis of the rest of the data by using the reaction limited colloidal aggregation model shows high correlation ($r^2 > 0.98$) for all concentrations of streptaviding used here (4−97 nM) with the results being presented in Table 3. Clearly, this model fits the experimental data over the large range of streptavidin concentrations, where aggregation of the nanoparticles was observed. In Table 3, ΔA_∞ represents the limiting absorbance value attained after aggregation and it is proportional to the mean number of bridge-forming bonds achieved per nanoparticles at the end of the reaction, b_∞. The values for ΔA_∞ were determined from the experimental data, where the signal leveled out at the end of the experiment or from the exponential fit with use of eq 3 (where it is assumed that ΔA is linearly proportional to b).

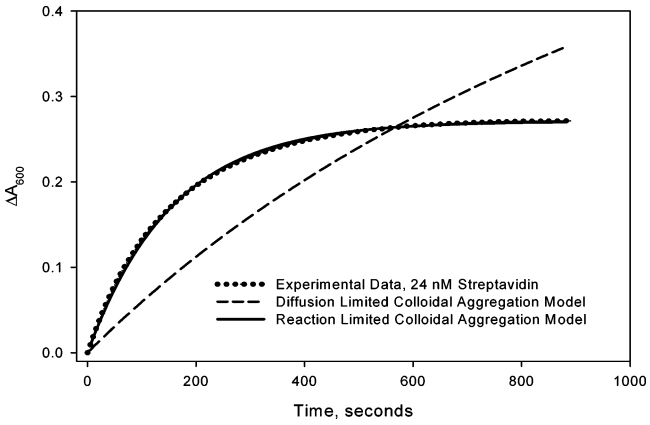

Figure 8. Change in absorbance at 600 nm with respect to time for 24 nM streptavidin (experimental data). Fits using diffusion-limited colloidal aggregation and reaction limited colloidal aggregation models.

TABLE 3: Physical Characterization of the Reaction Mixture Studied in Figure 4

streptavidin (S), nM	E = [S]/[BG][a]	$\Delta A_{\infty,fit}$[b]	$\Delta A_{\infty,exp}$[c]	τ_{sum}, s	r^2
4	5	1.91×10^{-3}	1.92×10^{-3}	526	0.984
8	10	0.119	0.118	3164	0.994
12	15	0.207	0.200	1652	0.997
16	20	0.357	0.355	410	0.999
20	25	0.381	0.377	416	0.999
24	30	0.335	0.341	150	0.999
32	35	0.293	0.293	102	0.999
53	66	0.267	0.274	100	0.988
97	122	0.038	0.040	1.2	0.988
196	244	ND	2.01×10^{-3}	ND[d]	ND[d]

[a] [BG] = concentration of biotinylated gold nanoparticles = 0.80 nM and is the same for all experiments. [b] $\Delta A_{\infty,fit}$ obtained from the exponential fit. [c] Experimental data. [d] Not determined.

The aggregation time constant, τ_{sum}, varied with the concentration of streptavidin. The largest value of τ_{sum} was observed between 8 and 12 nM streptavidin, which corresponds to the slowest aggregation of nanoparticles (Figure 4).

Conclusions

Surface modification of gold nanoparticles with ligands by using a simple technique was successfully accomplished. This technique led to preparations of stable biotinylated gold nanoparticles that were very effective in preventing nonspecific adsorption of proteins and allowing, at the same time, for

specific biomolecular recognition to occur. Biomolecule-mediated, controlled aggregation of biotinylated gold nanoparticles was induced by addition of streptavidin molecules in solution and the aggregation process was followed by optical absorption spectroscopy and TEM. Reversibility of aggregation, an important concept in determining that the process was mediated exclusively by specific molecular recognition, was accomplished by the addition of soluble biotin to the streptavidin−nanoparticle aggregates. This concept had not been demonstrated in other reports dealing with biotinylated gold nanoparticles.

The kinetic data for the interactions of streptavidin and biotinylated nanoparticles were analyzed by using a reaction-limited colloidal aggregation model to obtain quantitative information on the extent of streptavidin-induced aggregation of gold nanoparticles. Since these methods require the measurement of absorbance at only one wavelength using optical absorption spectroscopy, a simpler means of characterization of aggregation of metallic nanoparticles was achieved. This provided a more quantitative insight in the aggregation process with use of the semiempirical "flocculation parameter" and changes in absorbance.

Acknowledgment. We gratefully acknowledge the financial support for this project provided by the Armor College of Engineering and the Department of Chemical and Environmental Engineering at the Illinois Institute of Technology. XPS analysis of the samples was performed at National ESCA and Surface Analysis Center for Biomedical Problems at the University of Washington (NIH grant EB002027).

References and Notes

(1) Storhoff, J. J.; Elghanian, R.; Mucic, R. C.; Mirkin, C. A.; Letsinger, R. L. *J. Am. Chem. Soc.* **1998**, *120*, 1959−1964.

(2) Reynolds, R. A., III; Mirkin, C. A.; Letsinger, R. L. *J. Am. Chem. Soc.* **2000**, *122*, 3795−3796.

(3) Elghanian, R.; Storhoff, J. J.; Mucic, R. C.; Letsinger, R. L.; Mirkin, C. A. *Science* **1997**, *277*, 1078−1081.

(4) (a) Sastry, M.; Lala, N.; Patil, V.; Chavan, S. P.; Chittiboyina, A. G. *Langmuir* **1998**, *14*, 4138−4142. (b) Thanh, N. T. K.; Rosenzweig, Z. *Anal. Chem.* **2002**, *74*, 1624−1628.

(5) Cobbe, S.; Connolly, S.; Nagle, L.; Eritja, R.; Fitzmaurice, D.; Ryan, D. *J. Phys. Chem. B* **2003**, *107*, 470−477.

(6) Nath, N.; Chilkoti, A. *Anal. Chem.* **2002**, *74*, 504−509.

(7) Alvarez, M. M.; Khoury, J. T.; Schaaff, T. G.; Shafigullin, M. N.; Vezmar, I.; Whetten, R. L. *J. Phys. Chem. B* **1997**, *101*, 3706−3712.

(8) Collier, C. P.; Vossmeyer, T.; Heath, J. R. *Annu. Rev. Phys. Chem.* **1998**, *49*, 371−404.

(9) Wessels, J. M.; Nothofer, H.-G.; Ford, W. E.; von Wrochem, F.; Scholz, F.; Vossmeyer, T.; Schroedter, A.; Weller, H.; Yasuda, A. *J. Am. Chem. Soc.* **2004**, *126*, 3349−3356.

(10) Ulman, A. *An Introduction to Ultrathin Organic Films*: *from Langmuir−Blodgett to Self-Assembly*; Academic Press: Boston, MA, 1991.

(11) (a) Connolly, S.; Cobbe, S.; Fitzmaurice, D. J. *Phys. Chem. B.* **2001**, *105*, 2222−2226. (b) Connolly, S.; Rao, S. N.; Fitzmaurice, D. J. *Phys. Chem. B* **2000**, *104*, 4765−4776.

(12) (a) Chapman, R. G.; Ostuni, E.; Takayama, S.; Holmlin, R. E.; Yan, L.; Whitesides, G. M. *J. Am. Chem. Soc.* **2000**, *122*, 8303−8304. (b) Ostuni, E.; Chapman, R. G.; Holmlin, R. E.; Takayama, S.; Whitesides, G. M. *Langmuir* **2001**, *17*, 5605−5620.

(13) Aslan, K.; Pérez-Luna, V. H. *Langmuir* **2002**, *18*, 6059−6065.

(14) Weisbecker, C. S.; Merritt, M. G.; Whitesides, G. M. *Langmuir* **1996**, *12*, 3763−3772.

(15) Mayya, K. S.; Patil, V.; Sastry, M. *Langmuir* **1997**, *13*, 3944−3747.

(16) Mulvaney, P. *Langmuir* **1996**, *12*, 788−800.

(17) Pérez-Luna, V. H.; Aslan, K.; Betala, P. In *Encyclopedia of Nanoscience and Nanotechnology*; Nalwa H. S., Ed.; American Scientific Publishers: Stevenson Ranch, CA, 2004; Vol. 2, pp 27−49.

(18) Schmitt, J.; Mächtle, P.; Eck, D.; Möhwald, H.; Helm, C. A. *Langmuir* **1999**, *15*, 3256−3266.

(19) Eck, D.; Helm, C. A.; Wagner, N. J.; Vaynberg, K. A. *Langmuir* **2001**, *17*, 957−960.

(20) (a) Riepl, M.; Enander, K.; Liedberg, B.; Schaferling, M.; Kruschina, M.; Ortigao, F. *Langmuir* **2002**, *18*, 7016−7023. (b) Lahiri, J.; Isaacs, L.; Grzybowski, B.; Carbeck, J. D.; Whitesides, G. M. *Langmuir* **1999**, *15*, 7186−7198.

(21) Green, N. M. *Adv. Protein Chem.* **1975**, *29*, 85−133.

(22) Kreibig, U.; Althoff, A.; Pressmann, H. *Surf. Sci.* **1981**, *106*, 308−317.

(23) Quinten, M.; Kreibig, U. *Surf. Sci.* **1986**, *172*, 557−577.

(24) (a) Darst, S. A.; Ahlers, M.; Meller, P. H.; Kubalek, E. W.; Blankenburg, R.; Ribi, H. O.; Ringsdorf, H.; Kornberg, R. D. *Biophys. J.* **1991**, *59*, 387−396. (b) Häusling, L.; Michel, B.; Ringsdorf, H.; Rohrer, H. *Angew. Chem., Int. Ed. Engl.* **1991**, *30*, 569−572. (c) Weber, P. C.; Ohlendorf, D. H.; Wendoloski, J. J.; Salemme, F. R. *Science* **1989**, *243*, 85−88.

(25) (a) Schaaf, P.; Voegel, J.-C.; Senger, B. *J. Phys. Chem. B* **2000**, *104*, 2204−2214. (b) Feder, J. *J. Theor. Biol.* **1980**, *87*, 237. (c) Feder, J.; Giaever, J. *J. Colloid Interface Sci.* **1980**, *78*, 144.

(26) von Schultess, G. K.; Benedek, G. B.; De Blois R. W. *Macromolecules* **1983**, *16*, 434−440.

(27) Lynch, N. J.; Kilpatrick, P. K.; Carbonell, R. G. *Biotechnol. Bioeng.* **1996**, *50*, 151−168.

(28) Smoluchowski, M. *Z. Phys. Chem.* **1917**, *92*, 129−168.